Original Article | Neuroimaging and Head & Neck

eISSN 2005-8330
https://doi.org/10.3348/kjr.2022.0492
Korean J Radiol 2023;24(3):235-246

Korean Journal of Radiology
KJR

Tumor Habitat Analysis Using Longitudinal Physiological MRI to Predict Tumor Recurrence After Stereotactic Radiosurgery for Brain Metastasis

Da Hyun Lee[1], Ji Eun Park[2], NakYoung Kim[3], Seo Young Park[4], Young-Hoon Kim[5], Young Hyun Cho[5], Jeong Hoon Kim[5], Ho Sung Kim[2]

[1]Department of Radiology, Ajou University School of Medicine, Suwon, Korea
[2]Department of Radiology and Research Institute of Radiology, University of Ulsan College of Medicine, Asan Medical Center, Seoul, Korea
[3]DYNAPEX LLC, Seoul, Korea
[4]Department of Statistics and Data Science, Korea National Open University, Seoul, Korea
[5]Department of Neurosurgery, University of Ulsan College of Medicine, Asan Medical Center, Seoul, Korea

Objective: It is difficult to predict the treatment response of tissue after stereotactic radiosurgery (SRS) because radiation necrosis (RN) and tumor recurrence can coexist. Our study aimed to predict tumor recurrence, including the recurrence site, after SRS of brain metastasis by performing a longitudinal tumor habitat analysis.

Materials and Methods: Two consecutive multiparametric MRI examinations were performed for 83 adults (mean age, 59.0 years; range, 27–82 years; 44 male and 39 female) with 103 SRS-treated brain metastases. Tumor habitats based on contrast-enhanced T1- and T2-weighted images (structural habitats) and those based on the apparent diffusion coefficient (ADC) and cerebral blood volume (CBV) images (physiological habitats) were defined using k-means voxel-wise clustering. The reference standard was based on the pathology or Response Assessment in Neuro-Oncologycriteria for brain metastases (RANO-BM). The association between parameters of single-time or longitudinal tumor habitat and the time to recurrence and the site of recurrence were evaluated using the Cox proportional hazards regression analysis and Dice similarity coefficient, respectively.

Results: The mean interval between the two MRI examinations was 99 days. The longitudinal analysis showed that an increase in the hypovascular cellular habitat (low ADC and low CBV) was associated with the risk of recurrence (hazard ratio [HR], 2.68; 95% confidence interval [CI], 1.46–4.91; P = 0.001). During the single-time analysis, a solid low-enhancing habitat (low T2 and low contrast-enhanced T1 signal) was associated with the risk of recurrence (HR, 1.54; 95% CI, 1.01–2.35; P = 0.045). A hypovascular cellular habitat was indicative of the future recurrence site (Dice similarity coefficient = 0.423).

Conclusion: After SRS of brain metastases, an increased hypovascular cellular habitat observed using a longitudinal MRI analysis was associated with the risk of recurrence (i.e., treatment resistance) and was indicative of recurrence site. A tumor habitat analysis may help guide future treatments for patients with brain metastases.

Keywords: Radiosurgery; Brain metastasis; Response assessment; Tumor habitat; Radiation necrosis

INTRODUCTION

Stereotactic radiosurgery (SRS) is becoming a popular therapeutic option for brain metastases [1,2]; however, distinguishing radiation necrosis (RN) from tumor recurrence remains challenging. RN and tumor recurrence have common imaging findings, such as contrast enhancement, peritumoral edema, and a mass effect

Received: July 21, 2022 **Revised:** November 8, 2022 **Accepted:** December 11, 2022
Corresponding author: Ji Eun Park, MD, PhD, Department of Radiology and Research Institute of Radiology, University of Ulsan College of Medicine, Asan Medical Center, 88 Olympic-ro 43-gil, Songpa-gu, Seoul 05505, Korea.
• E-mail: jieunp@gmail.com

[3]. There is no definitive imaging technique that can accurately differentiate between these two entities [4,5]. Because both RN and tumor recurrence may coexist in SRS-treated tissue comprising a viable tumor, capillary damage, ischemia, and chemotherapy damage [4,6-8], a combination of diffusion- and perfusion-weighted MRI can provide useful information. Diffusion- and perfusion-weighted MRI have been confirmed as effective tools that can increase the diagnostic confidence [4,6,9,10], depict angiogenesis and necrotic tissue, and improve the diagnostic accuracy better than conventional MRI alone [11-13].

A tumor habitat analysis can distinguish subregions within a heterogeneous tumor by identifying similar voxels with common tumor biology [14,15]. A recent habitat analysis using structural MRI [16] showed that a habitat defined by low T2 and low T1 contrast-enhancing signal intensity was associated with viable tumors after SRS for brain metastases. Such a quantitative tumor habitat analysis may be helpful for assessing the residual tumor burden of metastatic tumors after treatment and determining the target for additional SRS. Nonetheless, this study was limited to cross-sectional anatomical MRI data. A previous radiological-pathological correlation analysis of 11 brain metastases treated with SRS revealed that a single MRI examination could not sufficiently determine pathological failure, but that serial MRI was practical for predicting the treatment response [17]. A longitudinal study using diffusion-weighted and dynamic susceptibility contrast (DSC) perfusion-weighted imaging, which reflect tumor cellularity and vascularity, may reveal effective tools that can predict treatment resistance and local recurrence sites.

We hypothesized that an evaluation of brain metastases after SRS using serial diffusion- and perfusion-weighted physiological MRI would be useful for predicting the treatment response by identifying subregions of recurrent tumors and treatment-induced changes, and that a spatial tumor habitat analysis would enable the identification of the recurrence site by clustering similar apparent diffusion coefficient (ADC) and cerebral blood volume (CBV) values. This study aimed to predict tumor recurrence (i.e., the treatment response) after SRS of brain metastases by performing a longitudinal tumor habitat analysis using MRI.

MATERIALS AND METHODS

Patient Population

After receiving approval from the Institutional Review Board of Asan Medical Center (IRB No. 2021-4701), this single-center, retrospective, clinical study was conducted according to the United States Health Insurance Portability and Accountability Act (HIPAA) regulations and the Declaration of Helsinki. The need for written informed consent was waived. Additionally, it was conducted in accordance with the Strengthening the Reporting of Observational Studies in Epidemiology (STROBE) statement [18].

Using our center's Redcap database of brain metastases, we identified 301 patients treated during January 1, 2014 to November 30, 2020; of those 301 patients, 212 who fulfilled the following criteria were first identified and evaluated: age older than 18 years; initially diagnosed with brain metastasis and underwent subsequent SRS; brain metastasis with a size of at least 1 x 1 cm^2; and a contrast-enhancing lesion (CEL) in the brain metastasis that could be analyzed. Their eligibility for study inclusion was further evaluated using the following criteria: the tumor was enlarged by more than 20% or at least 5 mm after SRS, resulting in clinical suspicion of tumor recurrence according to the response assessment in neuro-oncology brain metastases (RANO-BM) criteria; underwent follow-up MRI including diffusion-weighted imaging (DWI) and DSC perfusion-weighted imaging at least twice; the first follow-up MRI was performed within 6 months after SRS; and adequate follow-up examination results were available for the assessment of the treatment response. We excluded 129 patients for the following reasons: 39 patients had brain metastases that did not show a sufficient increase in size; 43 patients underwent the first follow-up MRI more than 6 months after SRS; 36 patients did not undergo follow-up MRI including DWI and DSC perfusion-weighted imaging at least twice; and 11 patients did not have adequate follow-up examination results to allow an assessment of the treatment response. Finally, 83 patients (mean age, 59.0 years; range, 27–82 years; 44 male and 39 female) with a total of 103 brain metastases were included. A flowchart of the patient inclusion process is shown in Figure 1. Clinical data were collected from the database of the Asan Medical Center. When multiple SRS-treated metastases were present, up to three of the largest lesions of each patient were included.

Definition of Progression: Reference Standard

At our institution, patients with brain metastases underwent follow-up assessments involving brain MRI every 2 or 3 months after the initial SRS for 1 or 2 years

https://doi.org/10.3348/kjr.2022.0492

Korean Journal of Radiology
KJR

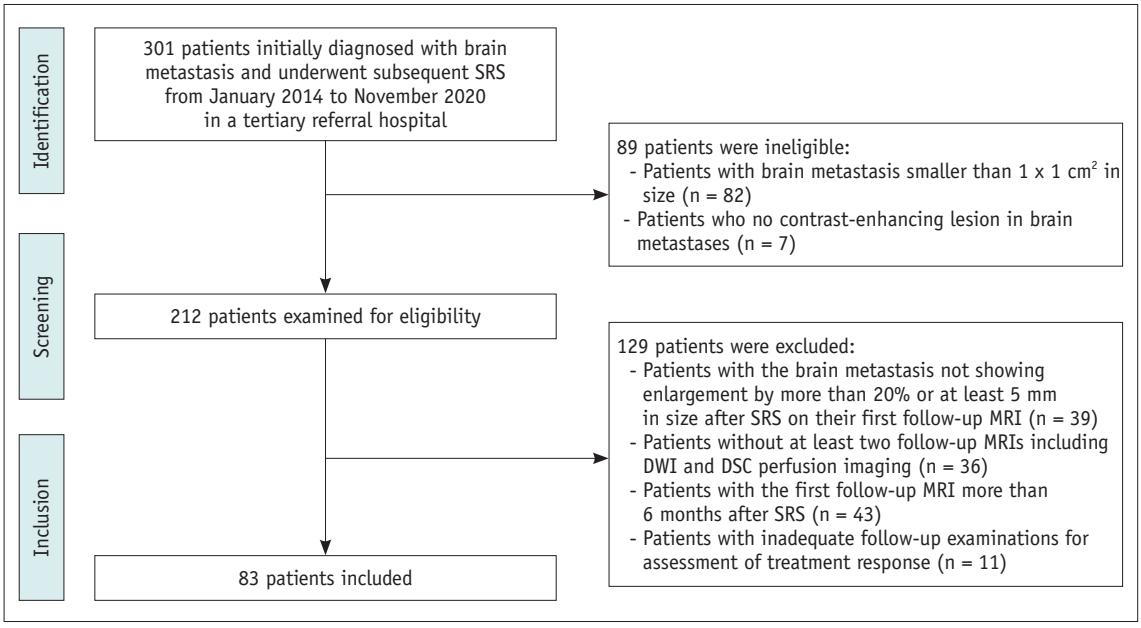

Fig. 1. Flowchart of the patient inclusion process. DSC = dynamic susceptibility contrast, DWI = diffusion-weighted imaging, SRS = stereotactic radiosurgery

during regular outpatient visits under the supervision of a multidisciplinary team [1,19]. If a patient developed a new symptom or if the neurological symptoms deteriorated, then MRI was performed regardless of the scheduled follow-up period. When clinically indicated, surgery was performed to confirm the final diagnosis of a viable tumor or RN. If surgery was not possible, then the viable tumor was determined using MRI in accordance with the RANO-BM criteria and serial follow-up examinations with intervals of at least 3 months were performed. Supplemental imaging examinations, such as 3,4-dihydroxy-6-[^{18}F]fluoro-L-phenylalanine) (^{18}F-DOPA) PET/CT, ^{11}C-methionine PET/CT, and ^{18}F-fluorodeoxyglucose (^{18}F-FDG) PET/CT, were also performed for individuals with equivocal MRI results. The clinicoradiological diagnosis was determined by a consensus reached during a multidisciplinary meeting involving three neurosurgeons (all with at least 15 years of experience with neuro-oncology) and two neuroradiologists (with 21 and 9 years of experience with neuro-oncologic imaging, respectively) who reviewed all imaging and medical records. When a CEL exhibited a steady increase in size during two or more successive follow-up MRI examinations within a 2- to 3-month interval and necessitated a change in treatment, the patient was classified as having tumor recurrence. The date of recurrence was recorded and the MRI examination was considered the confirmatory scan. In contrast, when a CEL subsequently regressed or became stable without a change in treatment within 6 months of the index imaging, the patient was categorized as having RN. The time to recurrence was defined as the time from SRS to the first local recurrence event.

MRI Acquisition

A 3T scanner was used for all MRI examinations (Ingenia 3.0 CX; Philips Healthcare). The following structural and physiological MRI sequences were performed: T2-weighted imaging (T2WI); fluid-attenuated inversion recovery (FLAIR) imaging; T1-weighted imaging (T1WI); DWI; DSC perfusion-weighted imaging; and three-dimensional (3D) contrast-enhanced (CE) T1WI.

The DWI parameters included the following: repetition time (TR)/echo time (TE), 3000/56 ms; diffusion gradient, b = 0 s/mm^2 and b = 1000 s/mm^2; field of view (FOV), 250 x 250 mm^2; matrix, 256 x 256; and slice thickness/gap, 5 mm/2 mm. The ADC values were calculated using DWI images with b = 1000 s/mm^2 and b = 0 s/mm^2. DSC perfusion-weighted imaging was performed using a gradient-echo echo-planar imaging protocol. A preload of 0.01 mmol/kg gadoterate meglumine was administered, followed by a dynamic bolus of a standard dose of 0.1 mmol/kg gadoterate meglumine (Dotarem; Guerbet) delivered at a rate of 4 mL/s using an MRI-compatible power injector (Spectris; Medrad). The contrast bolus was followed by 20 mL of saline at the same injection rate. The

 https://doi.org/10.3348/kjr.2022.0492

imaging parameters were as follows: TR/TE, 1808/40 ms; flip angle, 35°; FOV, 240 x 240 mm^2; slice thickness/gap, 5 mm/2 mm; matrix, 128 x 128; and total acquisition time, 1 minute and 54 seconds. Dynamic acquisition was performed at a temporal resolution of 1.5 seconds, and 60 dynamics were acquired.

Deep Learning-Based Segmentation of Contrast-Enhancing Lesions and Image Processing

Brain extraction was performed for 3D CE-T1WI and FLAIR imaging using an algorithm (https://github.com/MIC-DKFZ/HD-BET). Lesion segmentation was performed based on the images obtained using 3D CE-T1WI and FLAIR imaging and the 3D nnUNet-based algorithm (https://github.com/MIC-DKFZ/nnUNet) [20] of the PyTorch package version 1.1 of Python 3.7 (https://www.python.org). Because the CEL, necrosis, and peritumoral edema were segmented, only the CEL was included in the subsequent analysis. Hemorrhagic lesions were automatically excluded from the analysis if they showed similar hyperintensities on T1WI and CE-T1WI. The process was validated by an experienced neuroradiologist.

During T2WI and CE-T1WI, the signal intensity was normalized using kernel density estimation-based white matter segmentation [21] in R (version 4.1.1; Institute for Statistics and Mathematics; https://www.r-project.org/). To perform the DSC analysis, a pharmacokinetic map was computed using Nordic ICE (NordicNeuroLab). The quantity of blood (mL per 100 mL of tissue) was determined using the integrated DSC module, which combines a leakage correction algorithm of the relative CBV (rCBV) and manual noise thresholding. The Weisskoff–Boxerman method, which is based on the time-dependent deviation of the pixel-wise concentration-time curve from a reference curve, indicated that the leakage did not affect the estimations [22]. Normalized CBV (nCBV) maps were created by normalizing the rCBV maps in accordance with normal white matter.

To assess the changes in the follow-up examination results, the 3D CE-T1WI images of each patient in the dataset were co-registered and resampled into isometric voxels. Next, using rigid transformations with six degrees of freedom in the SPM package (version 12; https://www.fil.ion.ucl.ac.uk/spm/), the T2WI, nCBV, and ADC images were co-registered and resampled as isovoxel CE-T1WI images.

Tumor Habitat Analysis

The k-means clustering algorithm in scikit-learn (https://github.com/scikit-learn/scikit-learn) in Python 3.7 (https://www.python.org) was applied to aggregate the voxel clusters based on the signal intensities of T2WI and CE-T1WI or the values of nCBV and ADC reflecting functionally coherent subregions of the CEL. Using k-means clustering, samples from the dataset were classified as a given number of clusters with equal variances. Because the optimal number of clusters in a dataset is crucial to k-means clustering, three, four, and five clusters were initially evaluated (Supplementary Fig. 1).

Regarding the structural habitats, three clusters showed differences considering both T2WI and CE-T1WI results, whereas four and five clusters were identified by emphasizing the T2WI and CE-T1WI results, respectively. The four and five clusters displayed narrow ranges. Similarly, regarding the physiological habitats, three clusters demonstrated differences in both ADC and nCBV results, whereas four and five clusters with constrained ranges were identified by emphasizing the ADC and nCBV results, respectively. Therefore, based on the voxel-wise differences, three clusters were chosen to avoid overly parameterized models [16,23].

Structural habitats were defined as follows: an enhancing tissue habitat with high CE-T1 signal intensity irrespective of T2 signal intensity; a solid low-enhancing habitat with low T2 and CE-T1 signal intensity; and a nonviable tissue habitat with high T2 and low CE-T1 signal intensity. Low and high values were interpreted using the results of a data-driven analysis of k-means clustering without a specific threshold.

The ADC and CBV feature maps were used to define the following physiological habitats: a hypervascular cellular habitat with relatively low ADC and relatively high CBV values compared with other habitats; a hypovascular cellular habitat with relatively low ADC and CBV values; and a nonviable tissue habitat with relatively high ADC and relatively low CBV values.

The establishment of the tumor habitat is shown in Figure 2. For the longitudinal tumor habitat analysis, the differences in voxels in each habitat observed during the first and second examinations were calculated.

Analysis of the Recurrence Site

The recurrence site was analyzed using the tumor habitats established by the second follow-up examination and the confirmatory scan (MRI on the date of recurrence). The CEL at the recurrence site shown by the confirmatory scan was compared with the tumor habitats defined during

https://doi.org/10.3348/kjr.2022.0492

Korean Journal of Radiology
KJR

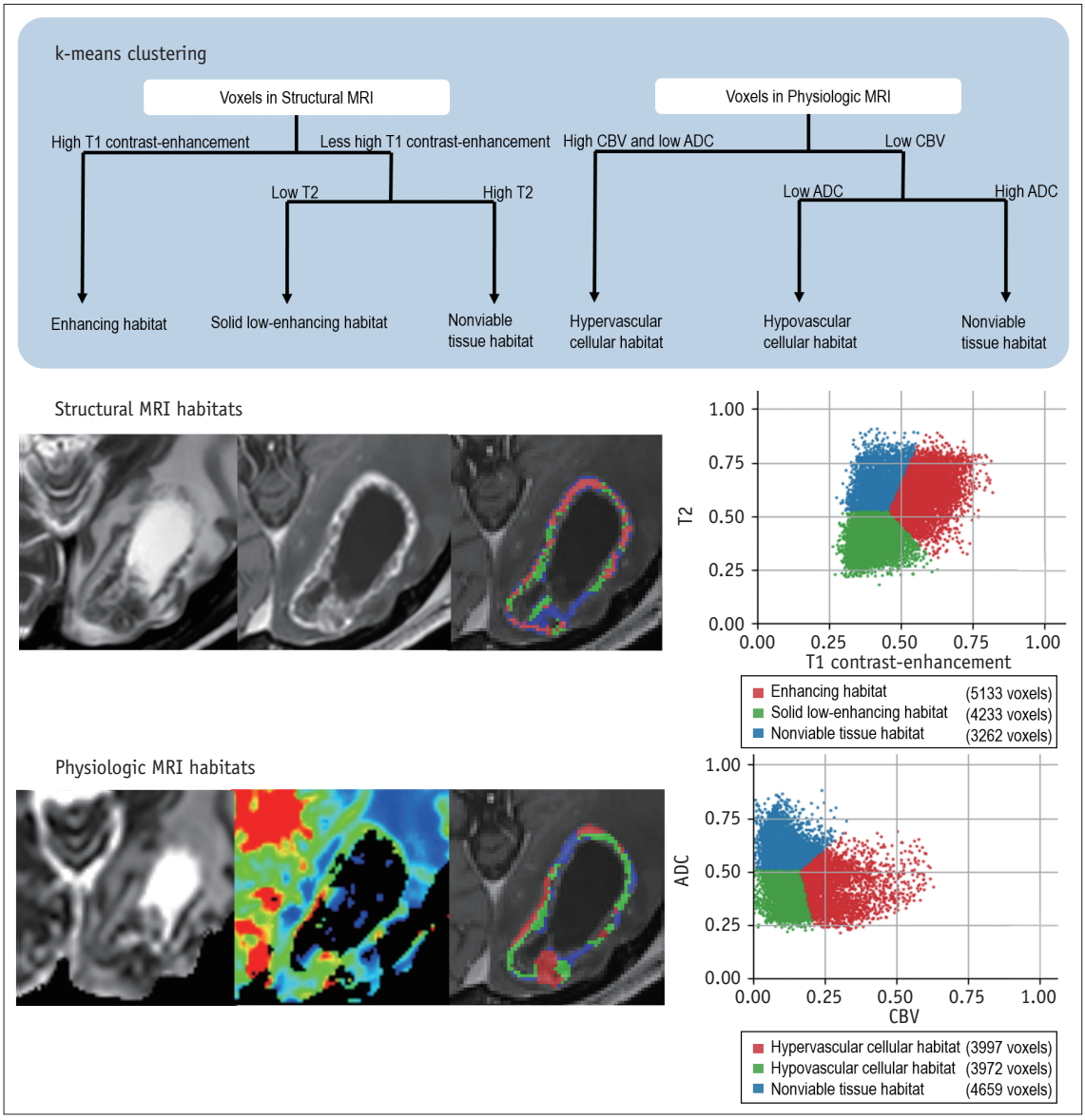

Fig. 2. Tumor habitats observed using structural MRI and physiological MRI to evaluate brain metastasis. To construct habitats using structural MRI, k-means clustering was applied for T2-weighted and contrast-enhanced T1-weighted images. To construct habitats using physiological MRI, k-means clustering was applied for ADC and CBV images. These images are of a 60-year-old male with colon cancer who was treated with stereotactic radiosurgery for metastasis in the left occipital lobe. Enhancing, solid low-enhancing, and nonviable tissue habitats are indicated by red, green, and blue subregions in the structural habitats, respectively. Similarly, hypervascular cellular, hypovascular cellular, and nonviable tissue habitats are represented by red, green, and blue subregions in the physiological habitats, respectively. ADC = apparent diffusion coefficient, CBV = cerebral blood volume

the second follow-up examination. The images obtained during the confirmatory scan were registered on the images obtained during the second follow-up examination. The region of interest of the CEL on the image obtained during the confirmatory scan was transferred to the tumor habitat observed during the second follow-up examination. The overlap of each habitat with the CEL at the time of recurrence was calculated using the Dice similarity coefficient ($\frac{2|H \cap R|}{|H| + |R|}$) [24], where H indicates each tumor habitat and R indicates the CEL at the time of recurrence. Briefly, the calculation is performed as follows: 2 (overlapped area between each tumor habitat at the second follow-up and CEL at the time of recurrence)/(sum of the tumor habitat at the second follow-up + CEL at the time of recurrence). The Dice similarity coefficient ranged from 0 (no overlap) to 1 (perfect agreement).

https://doi.org/10.3348/kjr.2022.0492

Statistical Analysis

The demographic characteristics of the patients were compared using the chi-square test or Fisher's exact test for discrete variables and the Student's *t* test for continuous variables.

A univariable analysis using Cox regression or the Kaplan–Meier method (log-rank test) was performed to analyze the associations of tumor habitats with the time to recurrence. The hazard ratios (HRs) indicate the relative change in the hazard incurred by a 1-unit increase in each parameter; during this study, 5000 voxels were considered one unit. A multivariable analysis was not performed because each tumor habitat was derived from a given CEL volume, resulting in mutual dependency among the tumor habitats and leading to multicollinearity in the regression analysis.

For the significant predictors identified by the univariable Cox regression, an optimal cutoff for stratifying groups at low risk and high risk for recurrence was estimated using maxstat in R (version 4.1.1; Institute for Statistics and Mathematics) with 10-fold cross-validation, which ensured unbiased prediction within the sample [25]. Because the z-score is the ratio of each regression coefficient to its standard error, the Wald statistic is the asymptotically standard normal when it is hypothesized that the corresponding β is zero [26]. These data were used to demonstrate the statistical significance of each spatiotemporal habitat type.

The R Statistical Package (version 4.1.1; Institute for Statistics and Mathematics) was used for all statistical analyses. Statistical significance was defined as $P < 0.05$.

RESULTS

Patient Characteristics

Eighty-three patients (mean age, 59.0 years; range, 27–82 years; 44 male and 39 female) with a total of 103 brain metastases who underwent longitudinal follow-up including MRI after SRS were enrolled in the study. Table 1 lists the characteristics of the patients and their brain metastases. The tumor recurrence and RN subgroups were not statistically significantly different in terms of age, sex, primary cancer origin, time interval between the detection of brain metastasis and SRS, time from SRS to the first and second imaging follow-up examinations, additional radiation therapy, combined chemotherapy, targeted therapy, steroid use, mean number of times SRS was performed, and metastasis size before and at the time of SRS. The time from SRS to the confirmatory scan was longer in the RN subgroup (mean ± standard deviation [SD], 508.2 ± 349.4 days) than in the tumor recurrence group (mean ± SD, 350.9 ± 150.9 days) ($P = 0.016$).

Table 1. Characteristics of the Patients and Their Metastatic Lesions

	Tumor Recurrence	Radiation Necrosis	*P*
Number of patients	34	49	
Age, years	60.0 ± 12.6	58.3 ± 10.5	0.508
Male	18 (53)	26 (53)	> 0.999
Primary cancer			0.199
Lung	20 (59)	28 (57)	
Breast	5 (15)	7 (14)	
Other	9 (26)	14 (29)	
Time from detection to SRS, days	19.5 ± 10.5	15.6 ± 9.7	0.090
SRS to first imaging follow-up, days	86.5 ± 34.1	83.0 ± 36.6	0.661
SRS to second imaging follow-up, days	178.7 ± 54.7	189.8 ± 79.3	0.482
SRS to confirmatory scan, days	350.9 ± 150.9	508.2 ± 349.4	0.016
Adjuvant therapy			0.223
Additional RT	0 (0)	1 (2)	
Combined with chemotherapy	4 (12)	1 (2)	
Targeted therapy	12 (35)	6 (12)	
Steroid usage	23 (68)	15 (28)	0.317
Number of metastatic lesions	37	66	
Mean dose of SRS, Gy*	28.4 ± 14.6	24.6 ± 15.2	0.223
Size prior to SRS, cm*	2.7 ± 1.1	2.8 ± 0.9	0.699
Size at time of SRS, cm*	2.8 ± 1.0	2.9 ± 1.0	0.730

Results are reported as the number (percent) or as mean ± standard deviation. *Data for metastatic lesions. RT = radiation therapy, SRS = stereotactic radiosurgery

Single-Time Analysis of the Tumor Habitat

The results of the univariable analysis performed to evaluate the associations between structural and physiological habitats and time to recurrence are summarized in Table 2. At the time of the first MRI examination, a solid low-enhancing habitat (low T2 and CE-T1 signal intensity) was associated with recurrence. Furthermore, a high number of voxels showing a solid low-enhancing structural habitat (HR, 1.54; 95% confidence interval [CI], 1.01–2.35; $P = 0.045$) were associated with recurrence. At the time of the second MRI examination, a

https://doi.org/10.3348/kjr.2022.0492

Korean Journal of Radiology
KJR

Table 2. Single Time Point Tumor Habitats and Their Associations with Recurrence of Brain Metastases After Stereotactic Radiosurgery

	Hazard Ratio	95% CI	*P*
First MRI			
Structural MRI habitats based on T2WI and CE-T1WI			
Enhancing tissue habitat	0.83	0.42–1.63	0.590
Solid low-enhancing habitat	1.54	1.01–2.35	0.045
Nonviable tissue habitat	0.45	0.14–1.50	0.195
Physiologic MRI habitats based on ADC and CBV			
Hypervascular cellular habitat	1.21	0.35–4.13	0.764
Hypovascular cellular habitat	0.70	0.30–1.61	0.401
Nonviable tissue habitat	1.06	0.67–1.69	0.799
Second MRI			
Structural MRI habitats based on T2WI and CE-T1WI			
Enhancing tissue habitat	0.97	0.50–1.89	0.927
Solid low-enhancing habitat	1.95	1.23–3.08	0.004
Nonviable tissue habitat	1.01	0.44–2.30	0.987
Physiologic MRI habitats based on ADC and CBV			
Hypervascular cellular habitat	20.1	2.90–139	0.002
Hypovascular cellular habitat	1.56	0.92–2.66	0.100
Nonviable tissue habitat	1.02	0.59–1.77	0.932

Hazard ratios reported here are for a 1 unit (5000 voxels) increase in each imaging parameter. ADC = apparent diffusion coefficient, CBV = cerebral blood volume, CE = contrast-enhanced, CI = confidence interval, T1WI = T1-weighted imaging, T2WI = T2-weighted imaging

high number of voxels showing either a solid low-enhancing structural habitat (HR, 1.95; 95% CI, 1.23–3.08; $P = 0.004$) or a hypervascular cellular physiological habitat (HR, 20.1; 95% CI, 2.90–139; $P = 0.002$) were associated with recurrence. The concordance index (C index) was 0.65 (95% CI, 0.55–0.75) for all statistically significant tumor habitats at a single time point.

Longitudinal Analysis of the Tumor Habitat: Recurrence Risk

The results of the longitudinal analysis of the tumor habitats are presented in Table 3. During the longitudinal analysis, an increase in the hypovascular cellular habitat was strongly associated with recurrence (HR, 2.68; 95% CI, 1.46–4.91; $P < 0.001$). The C index was 0.71 (95% CI, 0.62–0.80) after considering the changes in the hypovascular hypercellular habitat and all statistically significant tumor habitats at a single time point. Representative habitats of patients with SRS-treated metastasis with recurrence evaluated using longitudinal physiological MRI are shown in Figure 3 and Supplementary Figure 2.

Table 3. Longitudinal MRI Tumor Habitat Analysis and Associations with Recurrence of Brain Metastasis After Stereotactic Radiosurgery

Change in Tumor Habitat	Hazard Ratio	95% CI	*P*
Structural MRI habitats based on T2WI and CE-T1WI			
Enhancing tissue habitat	3.08	0.52–18.3	0.216
Solid low-enhancing habitat	1.64	0.75–3.61	0.215
Nonviable tissue habitat	1.92	0.82–4.48	0.133
Physiologic MRI habitats based on ADC and CBV			
Hypervascular cellular habitat	4.02	0.42–38.4	0.227
Hypovascular cellular habitat	2.68	1.46–4.91	< 0.001
Nonviable tissue habitat	0.70	0.18–2.76	0.607

Hazard ratios reported here are for a 1 unit (5000 voxels) increase in each imaging parameter. ADC = apparent diffusion coefficient, CBV = cerebral blood volume, CE = contrast-enhanced, CI = confidence interval, T1WI = T1-weighted imaging, T2WI = T2-weighted imaging

The optimal cutoff for the longitudinal physiological MRI evaluations of the habitats of groups at low risk and high risk for recurrence was an increase of more than 1345 voxels in the hypovascular cellular habitat. This cutoff separated the low- and high-risk groups, which were significantly different according to the log-rank test ($P < 0.001$). Supplementary Figure 3 shows the Kaplan–Meier survival curves of the groups at low risk and high risk for recurrence based on hypovascular cellular habitats.

Longitudinal Analysis of Tumor Habitat: Recurrence Sites

Thirty-seven lesions (35.9%; 37/103) were classified as tumor recurrence in 34 patients (41.0%; 34/83). The mean Dice similarity coefficient for the hypovascular cellular habitat observed using physiological MRI was the highest (0.423; range, 0.004–0.969; SD, 0.259), followed by the mean Dice similarity coefficient for the solid low-enhancing habitat observed using structural MRI (0.298; range, 0.015–0.942; SD, 0.247). Figure 4 shows the relationship between temporal changes in the hypovascular cellular habitats and the recurrence site.

DISCUSSION

We demonstrated that brain metastasis recurrence after SRS could be predicted by performing a longitudinal analysis involving diffusion- and perfusion-weighted physiological MRI of the tumor habitat. An increase in the hypovascular cellular habitat, which exhibits both low ADC and CBV values, was significantly associated with the time

https://doi.org/10.3348/kjr.2022.0492

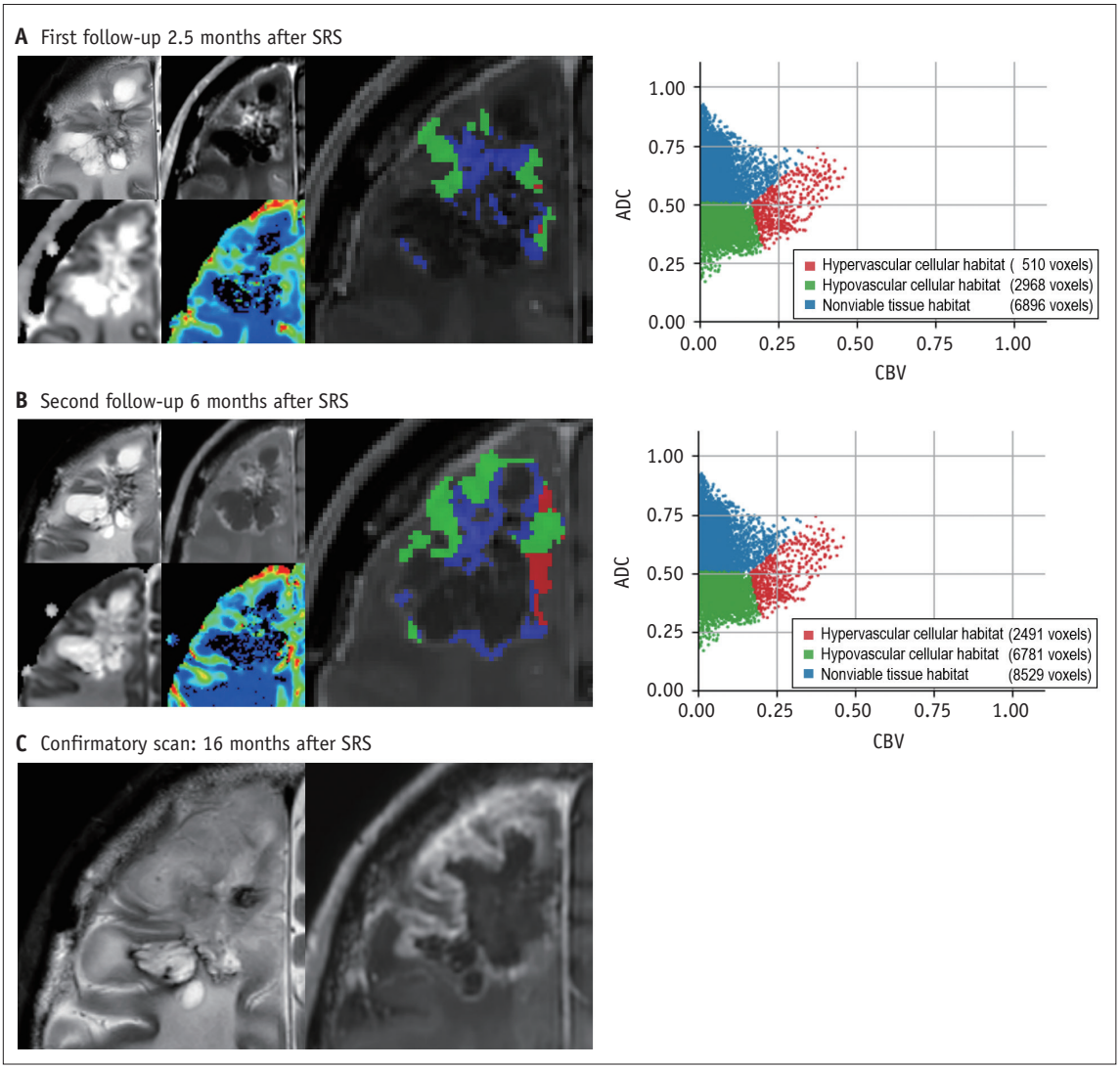

Fig. 3. Prediction of recurrence using a hypovascular cellular habitat. A 51-year-old male with brain metastasis attributable to lung cancer (adenocarcinoma) underwent whole brain radiotherapy and SRS of a lesion in the right frontal lobe. **A, B.** The longitudinal physiological MRI examination shows an increased hypovascular cellular habitat at the anterior aspect of the lesion and mild contrast enhancement. **C.** The confirmatory scan shows that the tumor progressed at the anterior aspect of the lesion. The time to recurrence was 16 months after SRS. ADC = apparent diffusion coefficient, CBV = cerebral blood volume, SRS = stereotactic radiosurgery

to recurrence of SRS-treated metastasis.

A tumor habitat analysis can identify distinct tumor subregions and cell populations that can be correlated with the biological state of the tissue by co-registering the images with histologic specimens [14,27]. We longitudinally analyzed tumor habitats using both physiological MRI and structural MRI for brain metastasis after SRS and compared their predictive values for recurrence. Structural MRI was found to be useful for the initial follow-up examination after SRS, during which a solid low-enhancing habitat (low T2 and CE-T1 signal intensity) was associated with recurrence. However, physiological MRI was helpful for predicting recurrence during the follow-up examinations and identified the tumor habitat that most closely matched the recurrence site. It was suggested that defining tumor subregions is helpful in radiation therapy planning, and the understanding of the spatial distribution of physiological tumor subregions could help optimize local radiotherapy [27,28]. Therefore, the hypovascular cellular subregion on images obtained with physiological MRI should be considered a target for further SRS or other local therapies.

When brain metastasis regrows after SRS, it is important to identify viable tumors that require follow-up imaging. Our study identified tumor habitats that could have viable tumors based on the findings of structural MRI and physiological MRI. These tumor habitats were solid

https://doi.org/10.3348/kjr.2022.0492

Korean Journal of Radiology
KJR

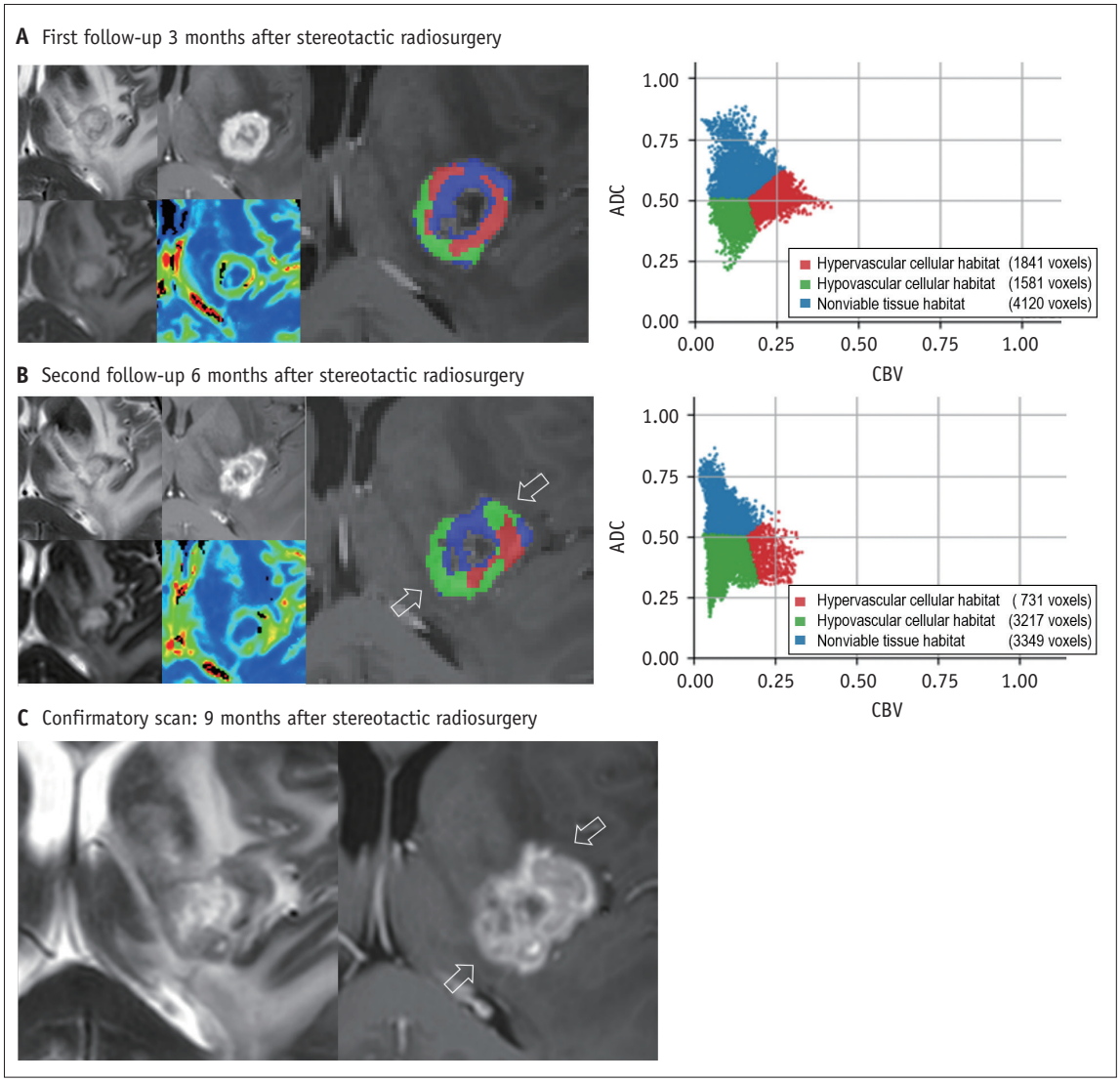

Fig. 4. Relationship between the increase in the hypovascular cellular habitat and recurrence site. A 64-year-old female with brain metastasis attributable to breast cancer. **A, B.** The longitudinal physiological MRI analysis shows that the hypovascular cellular habitat increased (from 1581 voxels to 3217 voxels) whereas the other habitats decreased. Spatial mapping shows an increase in the hypovascular cellular habitat at the medial and upper lateral aspects of the enhancing masses (arrows). **C.** Subsequently, the confirmatory scan performed during the 9-month follow-up examination shows that the hypovascular cellular habitat became the recurrence site (arrows). ADC = apparent diffusion coefficient, CBV = cerebral blood volume

low-enhancing with enhanced tissue on structural MRI and hypervascular cellular and hypovascular cellular on physiological MRI. Among them, the following habitats were associated with tumor recurrence at a single time point: solid low-enhancing habitat on structural MRI during the first and second follow-up examinations and hypervascular cellular on physiological MRI during the second follow-up examination. This suggests that viable tumors have inherent cellularity and a certain degree of vascularity. Accordingly, the aforementioned habitats may be potential prognostic factors for tumor recurrence. However, the predictive power for tumor recurrence cannot be guaranteed [29]. From the perspective of the longitudinal analysis, only changes in the hypovascular cellular habitat were associated with tumor recurrence, indicating that the cellularity of the viable tumor is an important factor that can determine tumor recurrence. Moreover, viable tumors can capture existing vessels or generate new ones [30,31]. However, the vasculature remains relatively low until vessel invasion [32]. Consequently, an increase in the hypovascular hypercellular habitat during longitudinal follow-up examinations might indicate a surge in viable tumors before vascular invasion.

https://doi.org/10.3348/kjr.2022.0492

Therefore, it could be used as a predictive biomarker to help determine the optimal additional therapy before overt tumor recurrence.

Importantly, we performed a habitat analysis of the CEL with both a solid low-enhancing habitat and a hypovascular cellular habitat within it. When the CEL and the solid portion and/or cellular portion with low T2 signal intensity were matched, tumor recurrence was indicated; however, when the CEL and solid portion and/or cellular portion were not matched, RN was indicated. Previous studies that used this interpretation found similar results. Using structural MRI, a T1/T2 mismatch, defined as nonmatching lesion boundaries on T2WI and CE-T1WI, showed 83.3% sensitivity and 91.1% specificity for RN [33]. Using physiological MRI, a layered appearance (without matching) consisting of outer, middle, and inner layers of high CBV, low ADC, and high ADC values, respectively, was suggestive of RN [34], with sensitivity and specificity rates of approximately 100% for 16 patients. Nonetheless, the visual analysis of enhancement patterns comprising T1/T2 signal intensity mismatch [35] or a layered appearance of high CBV, low ADC, and high ADC values with brain metastasis [36] is limited because it is a subjective assessment. In contrast, a quantitative tumor habitat analysis using k-means clustering applied to co-registered isometric voxels during our study provided objective and robust measurements that could be used to assess RN and viable tumors.

The hypovascular cellular habitat observed with physiological MRI had the highest mean Dice similarity coefficient (0.423; range, 0.004–0.969; SD, 0.259). The number of voxels of the CEL tended to change between the second follow-up examination and recurrence. Parametric response mapping [37], which monitors changes in a single voxel, provided an evaluation of the Dice similarity coefficient of the second follow-up examination and recurrence. Furthermore, parametric response mapping can be used to monitor each tumor habitat and determine the region matching the CEL at the time of recurrence, despite changes in tumor volume. As a result, rather than focusing on the actual number, a mean Dice similarity coefficient of 0.423 was utilized to determine the best tumor habitat corresponding to the recurrence site.

The number of patients with recurrent brain metastasis after SRS is likely to increase with improvements in systemic therapy [38]. The recent guidelines of the American Society of Clinical Oncology and the European Society of Clinical Oncology [1,38] recommend follow-up at 3-month intervals to diagnose brain metastasis recurrence, and that treatment should be continued according to the patient's performance status, neurological function, and prior treatment. A longitudinal analysis using a combination of diffusion- and perfusion-weighted MRI can predict [29] the timing of recurrence and stratify patients into groups at low risk and high risk for recurrence by defining hypovascular cellular habitats. The results of this assessment could be helpful in planning the next treatment option, especially localized therapy, surgery, or further SRS.

This study has several limitations. First, the strict pathological confirmation of image-based segmentation is difficult. Only a few patients underwent surgery for the recurrence of brain metastasis. Accurate localization of brain metastasis recurrence is limited because of the surgical difficulty. Nonetheless, we attempted to demonstrate that the recurrence site matched the tumor habitat by analyzing serial MRI examination results. It is essential to establish biologically validated habitat imaging as a promising research field [28,39,40] by continuing to perform research and applying those results to solid tumors [41,42]. Therefore, future studies are necessary to confirm the radiological and pathological correlations. Second, regarding structural MRI, the assignment of voxels to the enhancing habitat, solid low-enhancing habitat, or nonviable tissue habitat is based on logical assumptions. A tumor habitat analysis is a data-driven analysis that groups similar voxels within the CEL; however, this type of colocalization could be difficult to determine in clinical practice.

In conclusion, an increase in the hypovascular cellular habitat observed using longitudinal physiological MRI was associated with the risk of recurrence (i.e., treatment resistance) and was indicative of the recurrence site. These results may be helpful for monitoring patients after SRS and determining future localized therapeutic targets.

Supplement

The Supplement is available with this article at https://doi.org/10.3348/kjr.2022.0492.

Availability of Data and Material

The datasets generated or analyzed during the study are available from the corresponding author on reasonable request.

Korean Journal of Radiology
KJR

Conflicts of Interest

Ji Eun Park, Seo Young Park, and Ho Sung Kim who is on the editorial board of the *Korean Journal of Radiology* was not involved in the editorial evaluation or decision to publish this article. All remaining authors have declared no conflicts of interest.

Author Contributions

Conceptualization: Ji Eun Park. Data curation: Young-Hoon Kim, Young Hyun Cho, Jeong Hoon Kim. Formal analysis: Seo Young Park. Funding acquisition: Ji Eun Park. Investigation: Da Hyun Lee, Ji Eun Park, Young-Hoon Kim. Methodology: Ji Eun Park, NakYoung Kim. Project administration: Ji Eun Park. Resources: Da Hyun Lee, Young-Hoon Kim. Software: NakYoung Kim. Supervision: Ji Eun Park, Ho Sung Kim. Validation: Young Hyun Cho, Jeong Hoon Kim, Ho Sung Kim. Visualization: Da Hyun Lee, Ji Eun Park. Writing—original draft: Da Hyun Lee. Writing—review & editing: Ji Eun Park.

ORCID iDs

Da Hyun Lee
https://orcid.org/0000-0001-7593-0403
Ji Eun Park
https://orcid.org/0000-0002-4419-4682
NakYoung Kim
https://orcid.org/0000-0001-8756-8587
Seo Young Park
https://orcid.org/0000-0002-2702-1536
Young-Hoon Kim
https://orcid.org/0000-0002-8852-6503
Young Hyun Cho
https://orcid.org/0000-0002-3274-5096
Jeong Hoon Kim
https://orcid.org/0000-0001-7131-4523
Ho Sung Kim
https://orcid.org/0000-0002-9477-7421

Funding Statement

This research was supported by the Ministry of Health& Welfare, Republic of Korea (HI21C1161) and by a grant (2021IP0078) from the Asan Institute for Life Sciences, Asan Medical Center, Seoul, Korea.

REFERENCES

1. Le Rhun E, Guckenberger M, Smits M, Dummer R, Bachelot T, Sahm F, et al. EANO-ESMO clinical practice guidelines for diagnosis, treatment and follow-up of patients with brain metastasis from solid tumours. *Ann Oncol* 2021;32:1332-1347
2. Graber JJ, Cobbs CS, Olson JJ. Congress of neurological surgeons systematic review and evidence-based guidelines on the use of stereotactic radiosurgery in the treatment of adults with metastatic brain tumors. *Neurosurgery* 2019;84:E168-E170
3. Patel TR, McHugh BJ, Bi WL, Minja FJ, Knisely JP, Chiang VL. A comprehensive review of MR imaging changes following radiosurgery to 500 brain metastases. *AJNR Am J Neuroradiol* 2011;32:1885-1892
4. Chao ST, Ahluwalia MS, Barnett GH, Stevens GH, Murphy ES, Stockham AL, et al. Challenges with the diagnosis and treatment of cerebral radiation necrosis. *Int J Radiat Oncol Biol Phys* 2013;87:449-457
5. Kickingereder P, Dorn F, Blau T, Schmidt M, Kocher M, Galldiks N, et al. Differentiation of local tumor recurrence from radiation-induced changes after stereotactic radiosurgery for treatment of brain metastasis: case report and review of the literature. *Radiat Oncol* 2013;8:52
6. Shah R, Vattoth S, Jacob R, Manzil FF, O'Malley JP, Borghei P, et al. Radiation necrosis in the brain: imaging features and differentiation from tumor recurrence. *Radiographics* 2012;32:1343-1359
7. Rahmathulla G, Marko NF, Weil RJ. Cerebral radiation necrosis: a review of the pathobiology, diagnosis and management considerations. *J Clin Neurosci* 2013;20:485-502
8. Murphy ES, Xie H, Merchant TE, Yu JS, Chao ST, Suh JH. Review of cranial radiotherapy-induced vasculopathy. *J Neurooncol* 2015;122:421-429
9. Knitter JR, Erly WK, Stea BD, Lemole GM, Germano IM, Doshi AH, et al. Interval change in diffusion and perfusion MRI parameters for the assessment of pseudoprogression in cerebral metastases treated with stereotactic radiation. *AJR Am J Roentgenol* 2018;211:168-175
10. Sawlani V, Davies N, Patel M, Flintham R, Fong C, Heyes G, et al. Evaluation of response to stereotactic radiosurgery in brain metastases using multiparametric magnetic resonance imaging and a review of the literature. *Clin Oncol (R Coll Radiol)* 2019;31:41-49
11. Barajas RF, Chang JS, Sneed PK, Segal MR, McDermott MW, Cha S. Distinguishing recurrent intra-axial metastatic tumor from radiation necrosis following gamma knife radiosurgery using dynamic susceptibility-weighted contrast-enhanced perfusion MR imaging. *AJNR Am J Neuroradiol* 2009;30:367-372
12. Hoefnagels FW, Lagerwaard FJ, Sanchez E, Haasbeek CJ, Knol DL, Slotman BJ, et al. Radiological progression of cerebral metastases after radiosurgery: assessment of perfusion MRI for differentiating between necrosis and recurrence. *J Neurol* 2009;256:878-887
13. Mitsuya K, Nakasu Y, Horiguchi S, Harada H, Nishimura T, Bando E, et al. Perfusion weighted magnetic resonance imaging to distinguish the recurrence of metastatic brain tumors from radiation necrosis after stereotactic radiosurgery.

J Neurooncol 2010;99:81-88
14. O'Connor JP, Rose CJ, Waterton JC, Carano RA, Parker GJ, Jackson A. Imaging intratumor heterogeneity: role in therapy response, resistance, and clinical outcome. *Clin Cancer Res* 2015;21:249-257
15. Dextraze K, Saha A, Kim D, Narang S, Lehrer M, Rao A, et al. Spatial habitats from multiparametric MR imaging are associated with signaling pathway activities and survival in glioblastoma. *Oncotarget* 2017;8:112992-113001
16. Lee DH, Park JE, Kim N, Park SY, Kim YH, Cho YH, et al. Tumor habitat analysis by magnetic resonance imaging distinguishes tumor progression from radiation necrosis in brain metastases after stereotactic radiosurgery. *Eur Radiol* 2022;32:497-507
17. Sakuramachi M, Igaki H, Ikemura M, Yamashita H, Okuma K, Sekiya N, et al. Detection of residual metastatic tumor in the brain following gamma knife radiosurgery using a single or a series of magnetic resonance imaging scans: an autopsy study. *Oncol Lett* 2017;14:2033-2040
18. von Elm E, Altman DG, Egger M, Pocock SJ, Gøtzsche PC, Vandenbroucke JP; STROBE Initiative. The strengthening the reporting of observational studies in epidemiology (STROBE) statement: guidelines for reporting observational studies. *Lancet* 2007;370:1453-1457
19. National Comprehensive Cancer Network. NCCN clinical practice guidelines in oncology. Central nervous system cancers, version 3.2020. *J Natl Compr Canc Netw* 2020;18:1537-1570
20. Isensee F, Schell M, Pflueger I, Brugnara G, Bonekamp D, Neuberger U, et al. Automated brain extraction of multisequence MRI using artificial neural networks. *Hum Brain Mapp* 2019;40:4952-4964
21. Reinhold JC, Dewey BE, Carass A, Prince JL. Evaluating the impact of intensity normalization on MR image synthesis. *Proc SPIE Int Soc Opt Eng* 2019;10949:109493H
22. Weisskoff R, Boxerman J, Sorensen A, Kulke S, Campbell T, Rosen B. Simulataneous blood volume and permeability mapping using a single Gd-based contrast injection. Proceedings of the Society of Magnetic Resonance, Second Annual Meeting; 1994 Aug 6-12; San Francisco, CA, USA: SMR, 1994. p.279
23. Gull SF. *Bayesian inductive inference and maximum entropy*. In: Erickson GJ, Smith CR, eds. *Maximum-entropy and Bayesian methods in science and engineering*. Dordrecht: Springer, 1988:53-74
24. Dice LR. Measures of the amount of ecologic association between species. *Ecology* 1945;26:297-302
25. Ingrisch M, Schneider MJ, Nörenberg D, Negrao de Figueiredo G, Maier-Hein K, Suchorska B, et al. Radiomic analysis reveals prognostic information in T1-weighted baseline magnetic resonance imaging in patients with glioblastoma. *Invest Radiol* 2017;52:360-366
26. Fox J, Weisberg S. *Cox proportional-hazards regression for survival data. An R and S-PLUS companion to applied regression*. New York: SAGE Publications, Inc., 2002
27. Tomaszewski MR, Gillies RJ. The biological meaning of radiomic features. *Radiology* 2021;298:505-516
28. Enderling H, Alfonso JCL, Moros E, Caudell JJ, Harrison LB. Integrating mathematical modeling into the roadmap for personalized adaptive radiation therapy. *Trends Cancer* 2019;5:467-474
29. Ballman KV. Biomarker: predictive or prognostic? *J Clin Oncol* 2015;33:3968-3971
30. Gavrilovic IT, Posner JB. Brain metastases: epidemiology and pathophysiology. *J Neurooncol* 2005;75:5-14
31. Eichler AF, Chung E, Kodack DP, Loeffler JS, Fukumura D, Jain RK. The biology of brain metastases-translation to new therapies. *Nat Rev Clin Oncol* 2011;8:344-356
32. Liu Q, Zhang H, Jiang X, Qian C, Liu Z, Luo D. Factors involved in cancer metastasis: a better understanding to "seed and soil" hypothesis. *Mol Cancer* 2017;16:176
33. Kano H, Kondziolka D, Lobato-Polo J, Zorro O, Flickinger JC, Lunsford LD. T1/T2 matching to differentiate tumor growth from radiation effects after stereotactic radiosurgery. *Neurosurgery* 2010;66:486-491; discussion 491-492
34. Cha J, Kim ST, Kim HJ, Kim HJ, Kim BJ, Jeon P, et al. Analysis of the layering pattern of the apparent diffusion coefficient (ADC) for differentiation of radiation necrosis from tumour progression. *Eur Radiol* 2013;23:879-886
35. Stockham AL, Tievsky AL, Koyfman SA, Reddy CA, Suh JH, Vogelbaum MA, et al. Conventional MRI does not reliably distinguish radiation necrosis from tumor recurrence after stereotactic radiosurgery. *J Neurooncol* 2012;109:149-158
36. Hainc N, Alsafwani N, Gao A, O'Halloran PJ, Kongkham P, Zadeh G, et al. The centrally restricted diffusion sign on MRI for assessment of radiation necrosis in metastases treated with stereotactic radiosurgery. *J Neurooncol* 2021;155:325-333
37. Galbán CJ, Chenevert TL, Meyer CR, Tsien C, Lawrence TS, Hamstra DA, et al. Prospective analysis of parametric response map-derived MRI biomarkers: identification of early and distinct glioma response patterns not predicted by standard radiographic assessment. *Clin Cancer Res* 2011;17:4751-4760
38. Vogelbaum MA, Brown PD, Messersmith H, Brastianos PK, Burri S, Cahill D, et al. Treatment for brain metastases: ASCO-SNO-ASTRO guideline. *J Clin Oncol* 2022;40:492-516
39. Sala E, Mema E, Himoto Y, Veeraraghavan H, Brenton JD, Snyder A, et al. Unravelling tumour heterogeneity using next-generation imaging: radiomics, radiogenomics, and habitat imaging. *Clin Radiol* 2017;72:3-10
40. Napel S, Mu W, Jardim-Perassi BV, Aerts HJWL, Gillies RJ. Quantitative imaging of cancer in the postgenomic era: radio(geno)mics, deep learning, and habitats. *Cancer* 2018;124:4633-4649
41. Crispin-Ortuzar M, Gehrung M, Ursprung S, Gill AB, Warren AY, Beer L, et al. Three-dimensional printed molds for image-guided surgical biopsies: an open source computational platform. *JCO Clin Cancer Inform* 2020;4:736-748
42. Kazerouni AS, Hormuth DA 2nd, Davis T, Bloom MJ, Mounho S, Rahman G, et al. Quantifying tumor heterogeneity via MRI habitats to characterize microenvironmental alterations in HER2+ breast cancer. *Cancers (Basel)* 2022;14:1837

https://doi.org/10.3348/kjr.2022.0492